Electronic Supplementary Material (ESI) for ChemComm.
This journal is © The Royal Society of Chemistry 2023

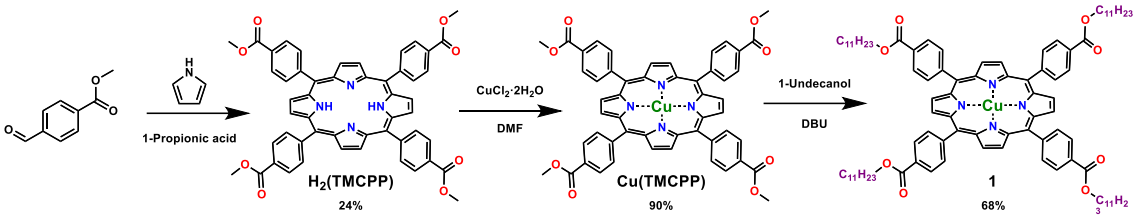

Scheme S1. Synthesis of **1**.

Synthesis of H_2(TMCPP)

4-(Methoxycarbonyl)benzaldehyde (1.7 g, 0.010 mol) was dissolved in 1-propionic acid (52 mL), to which pyrrole (0.73 mL, 0.011 mol) was added dropwise. The reaction mixture was refluxed for 2 hours. After cooling to room temperature, ca. 80 mL of acetone was added to the reaction mixture to afford the precipitate, which was collected by vacuum filtration and washed with acetone (0.527 g, 24%).

^{1}H NMR (400 MHz, $CDCl_3$, TMS): δ 8.91 (s, 8H), 8.44 (d, 8H), 8.29 (d, 8H), 4.11 (s, 12H), 2.81 (s, 2H).

MALDI-TOF MS (Matrix: HABA): Calcd. for $[C_{52}H_{38}N_4O_8H]^+$: m/z = 847.28. Found: 847.12.

Synthesis of Cu(TMCPP)

The mixture of H_2(TMCPP) (240 mg, 0.28 mmol), $CuCl_2 \cdot 2H_2O$ (604 mg, 3.54 mmol) and DMF (30 mL) was refluxed for 6 hours. After cooling to room temperature, the water was added to the reaction mixture to afford the precipitate, which was collected by vacuum filtration and washed with water. The precipitate was dissolved in CH_2Cl_2 and washed with water using separatory funnel for 3 times. The CH_2Cl_2 layer was dried over $MgSO_4$, and the solvent was evaporated to dryness. Recrystallization using CH_2Cl_2 and ethanol afforded purplish red powder of Cu(TMCPP) (232 mg, 90%).

^{1}H NMR (400 MHz, $CDCl_3$, TMS): δ 8.20 (broad signal), 4.04 (s).

MALDI-TOF MS (Matrix: HABA): Calcd. for $[CuC_{52}H_{36}N_4O_8]^+$: m/z = 906.96. Found: 907.18.

Synthesis of **1**

The mixture of Cu(TMCPP) (101 mg, 0.11 mmol), 1-undecanol (2 mL) and DBU (80 μL) was stirred at 180 °C for 12 hours under N_2 atmosphere. After cooling to room temperature, the excess methanol (ca. 30 mL) was added to the reaction mixture to afford the precipitate, which was collected by vacuum filtration and washed with methanol. The precipitate was purified using with the silica gel column chromatography with CH_2Cl_2 as the eluent. Recrystallization using CH_2Cl_2 and ethanol afforded purplish red crystals of Cu(TMCPP) (111 mg, 68%).

^{1}H NMR (400 MHz, $CDCl_3$, TMS):δ 8.214 (broad signal, 6.38H), 4.431 (broad signal, 7.26H), 1.855 (broad signal, 8.23H), 1.276-1.520 (broad signal, 68.93H), 0.871 (broad signal, 12H).
MALDI-TOF MS (Matrix: HABA): Calcd. for $[C_{92}H_{116}N_4O_8Cu]^+$: m/z = 1468.81. Found: 1468.64.
CHN elemental analysis calcd. (%) for $C_{92}H_{116}N_4O_8Cu$: C 75.20, H 7.96, N 3.81; found: C 75.202, H 7.949, N 3.994.

Physical property measurement

SCXRD analyses were performed using a Rigaku Varimax Saturn diffractometer. Diffraction data were processed using CrysAlisPro 4.0. The initial structures were obtained using SHELXT (2018/3) and refined with SHELXL (2018/3)[1] combined with Yadokari-XG.[2] PXRD measurements were performed on a Bruker D2 PHASER. PXRD patterns were simulated using Mercury 4.[3] DSC measurements were performed at heating and cooling rates of 10 K min^{-1} from 123 K to 298 K on a PerkinElmer DSC8500 under a flow of He gas (20 mL min^{-1}). ^{1}H NMR measurements were performed on JEOL AL-400 and the data was processed using JEOL Delta NMR software package. MALDI-TOF mass spectroscopy was performed on Shimadzu AXIMA Performance using 4'-hydroxyazobenzene-2-carboxylic acid (HABA) as the matrix, and the data was processed using mMass.[4] The elemental analysis was performed at the Research and Analytical Center for Giant Molecules, Tohoku University. Magnetic measurements were performed using a Quantum Design Physical Property Measurement System (PPMS) equipped with the ACMS option and a Quantum Design Magnetic Property Measurement System (MPMS). Energy framework analysis was performed using CrystalExplorer 21 at HF/3-21G level.[5] The Cu^{2+} ion was replaced by Ni^{2+} to avoid the effect of spin during calculations.

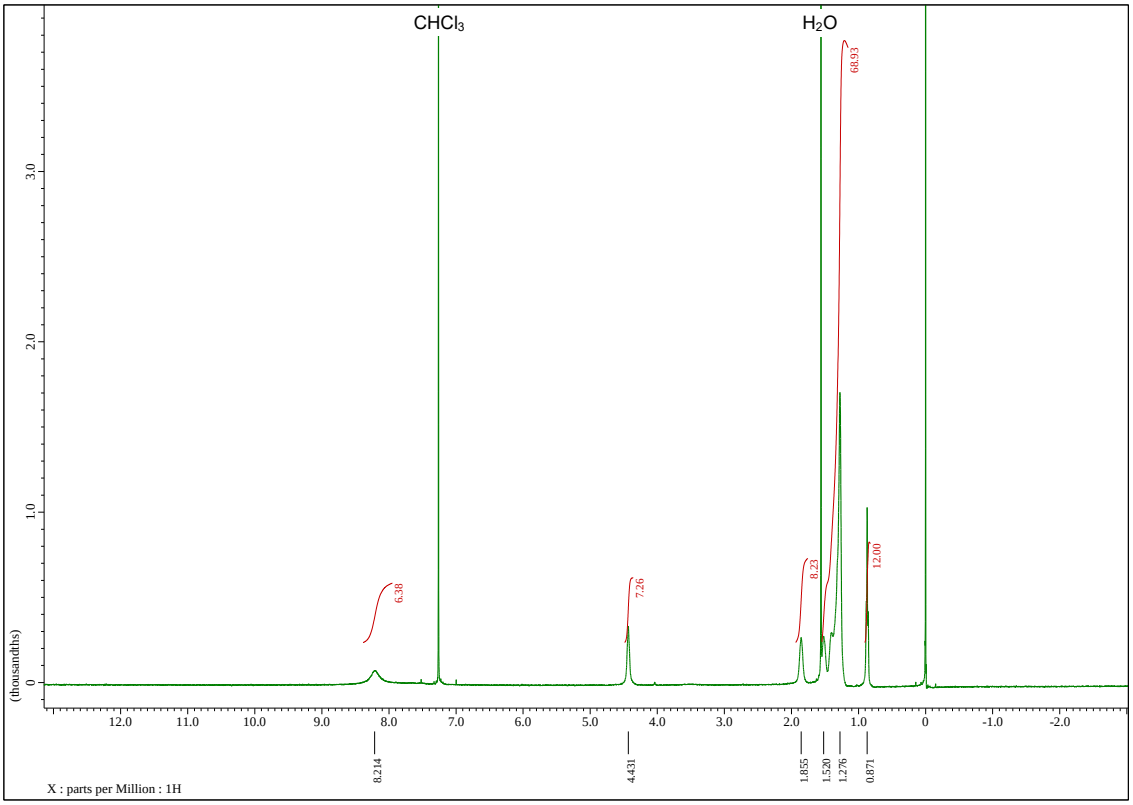

Fig. S1. ^{1}H NMR for **1** in $CDCl_3$. Paramagnetic spin of Cu^{2+} ion causes the signal broadening and deviation of integration values from the theoretical values.

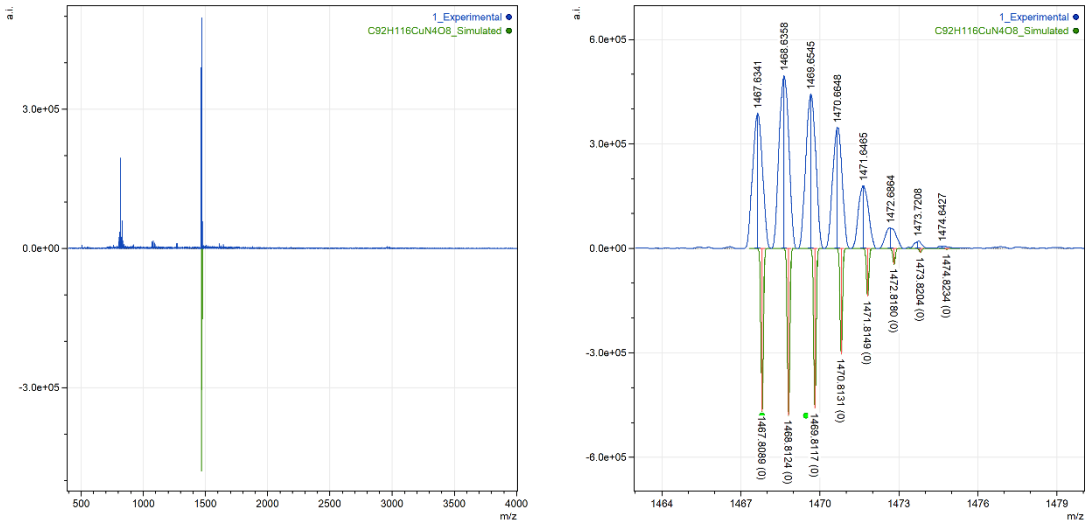

Fig. S2. MALDI-TOF MS spectra (experimental: above, simulated: below) for **1**.

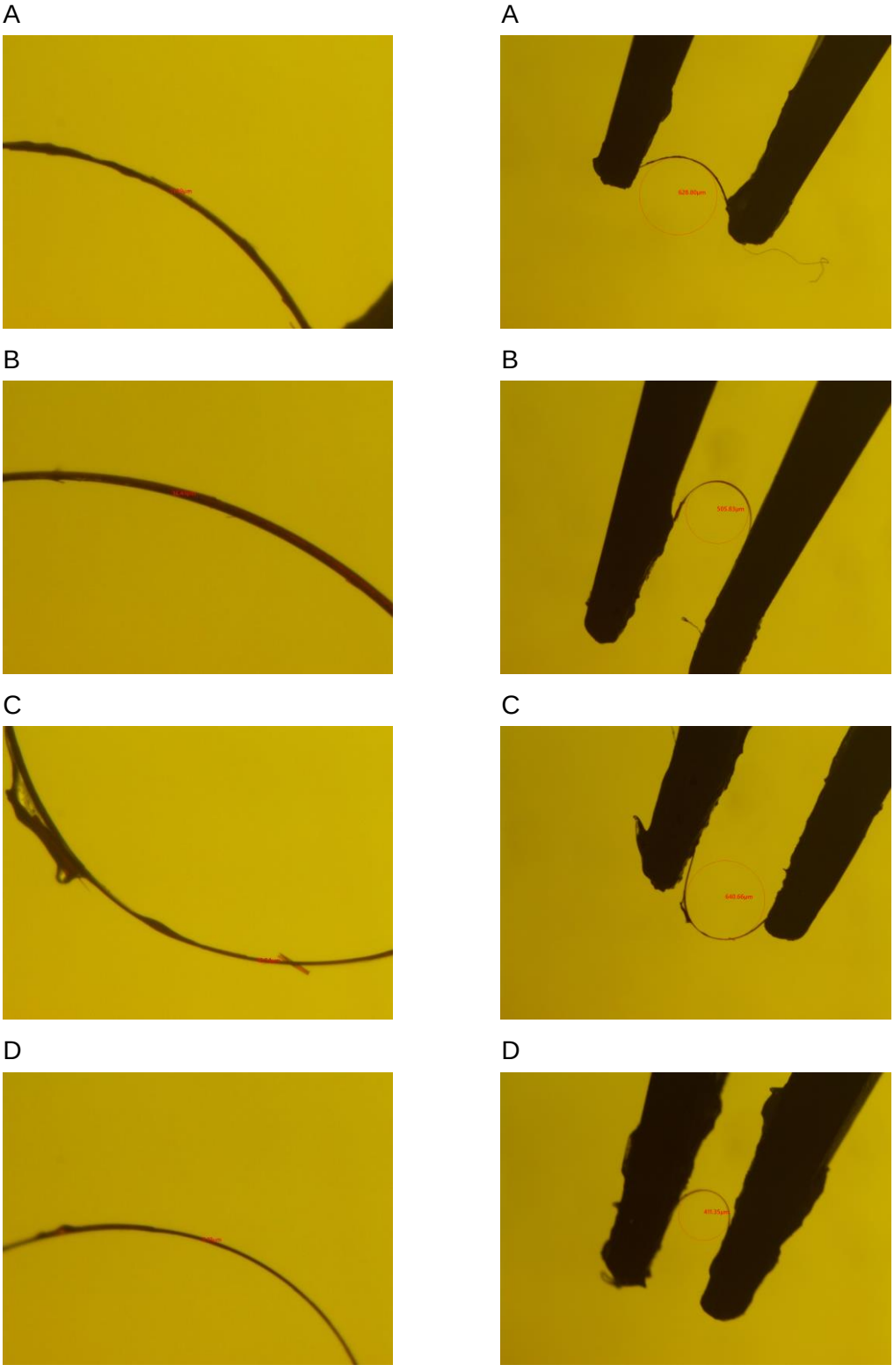

Fig. S3-1. Thickness (left) and radius of the bending loop (right) of **1** used for strain measurements.

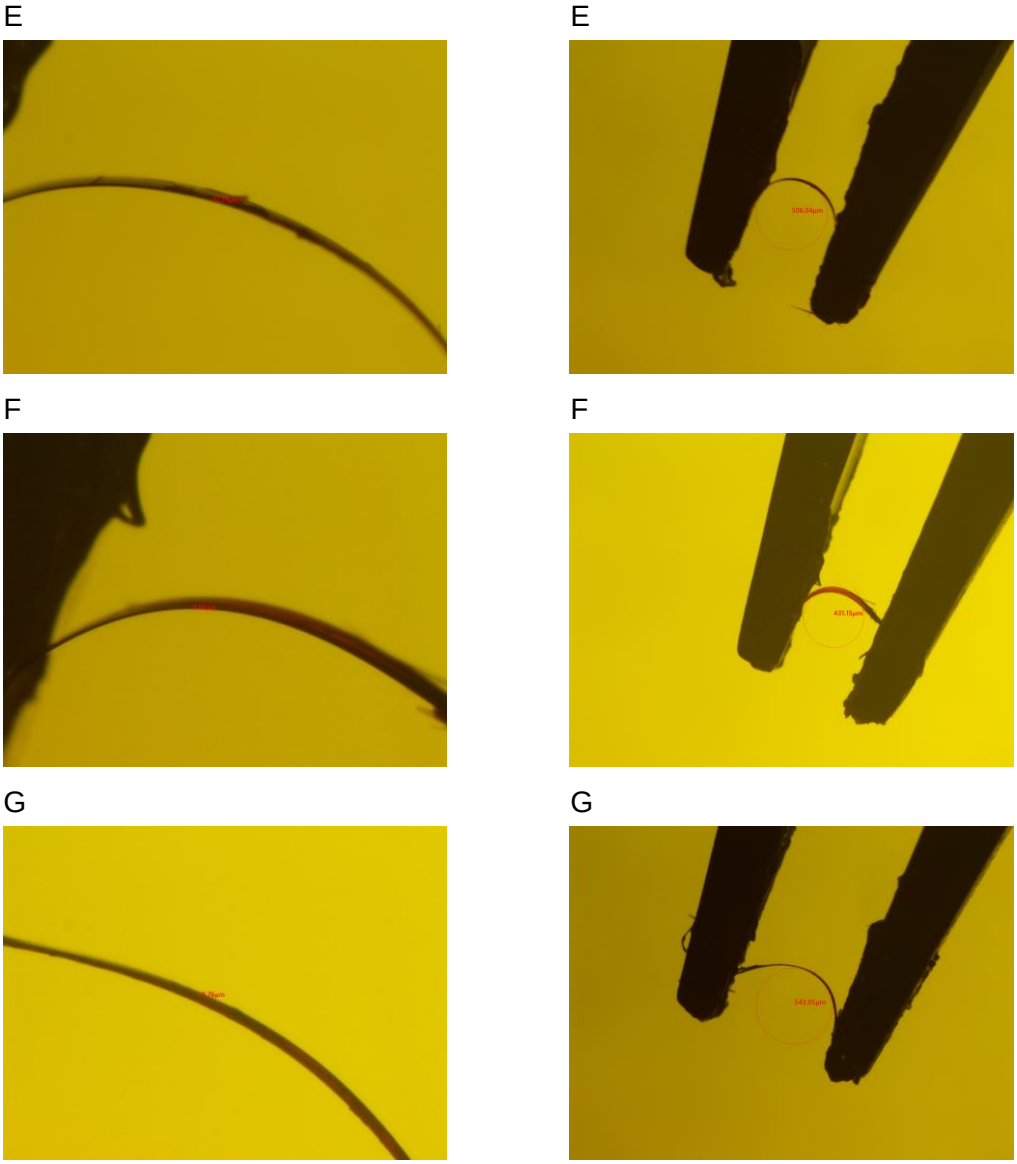

Fig. S3-2. Thickness (left) and radius of the bending loop (right) of **1** used for strain measurements.

Table S1. Thickness, radius of the bending loop and bending strain of **1**.

	Thickness / µm	Radius / µm	Bending strain / %
A	11.89	628.80	1.89
B	14.45	505.83	2.86
C	10.84	640.66	1.69
D	8.19	411.35	1.99
E	12.74	506.04	2.51
F	11.96	431.15	2.77
G	9.76	543.05	1.80
Average			2.2(5)

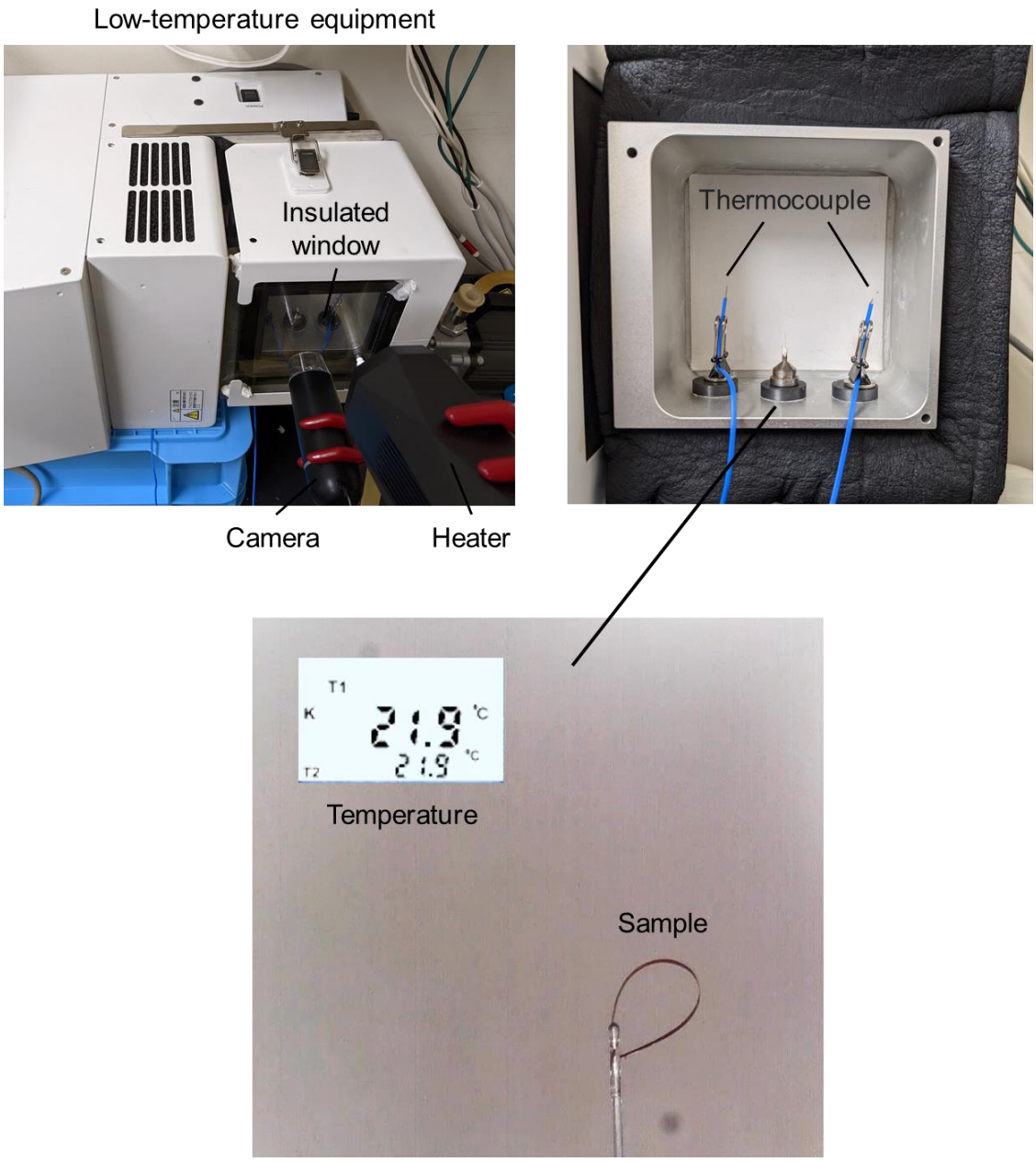

Fig. S4. Cooling of the loop of **1** using low temperature equipment. The temperature was measured using two thermocouples. During the cooling, the temperature diffecence in the two thermocouples are less than 0.8 K. This appartus cools the sample using natural convection, making it possible to avoid the deformation of the sample due to flow of the cold gas. In this setup, the lowest available temperature is ca. 200 K.

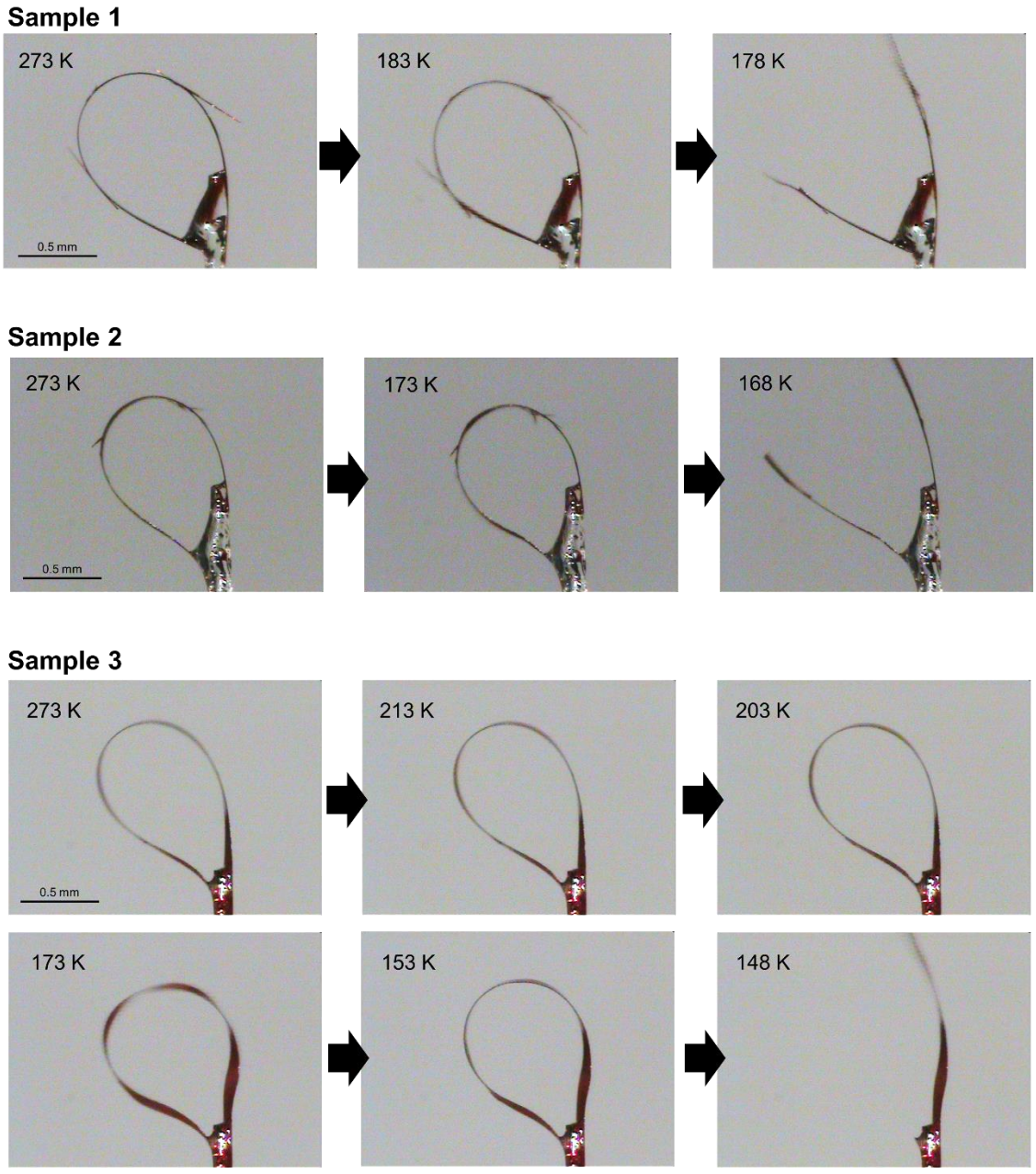

Fig. S5. Cooling of the loops of **1** under cold stream of N_2 gas.

Table S2. Crystalline cell parameters for **1**.

	1	**1**	**1**	**1**
T / K	273	213	153	123
Formula	$C_{92}H_{116}CuN_4O_8$	$C_{92}H_{116}CuN_4O_8$	$C_{92}H_{116}CuN_4O_8$	$C_{92}H_{116}CuN_4O_8$
Crystal system	Triclinic	Triclinic	Triclinic	Triclinic
Space group	*P*-1	*P*-1	*P*-1	*P*-1
Z	2	2	2	2
a / Å	9.6256(4)	9.5607(4)	9.2898(6)	9.2061(4)
b / Å	17.1012(5)	17.0874(6)	17.0160(6)	16.8734(6)
c / Å	25.3585(8)	25.5066(9)	25.7914(12)	25.5653(7)
α / °	86.855(2)	86.571(3)	88.749(3)	89.054(3)
β / °	84.389(3)	84.392(3)	82.945(5)	83.014(3)
γ / °	80.138(3)	79.360(3)	81.204(4)	81.318(3)
V / Å^3	4089.8(2)	4072.0(3)	3998.5(4)	3896.6(2)
ρ / g cm^{-3}	1.193	1.198	1.220	1.252
GOF	1.018	1.016	0.981	1.020
R_1(gt)	0.0693	0.0793	0.0842	0.0830
wR_2(gt)	0.1748	0.1684	0.1704	0.2104
R_1(all)	0.1142	0.1645	0.1777	0.1253
wR_2(ref)	0.2044	0.2167	0.2267	0.2897
CCDC number	2293139	2293140	2293141	2293142

Table S3. *T*-dependence of the crystalline cell parameters for **1**.

T / K	*a* / Å	*b* / Å	*c* / Å	*α* / °	*β* / °	*γ* / °	*V* / Å^3
293	9.665(2)	17.132(4)	25.337(10)	87.1(2)	84.4(2)	80.25(2)	4112(2)
283	9.6481(18)	17.117(4)	25.332(10)	87.01(3)	84.36(2)	80.132(18)	4099(2)
273	9.6277(17)	17.099(4)	25.348(10)	86.93(2)	84.36(2)	80.037(17)	4087(2)
263	9.6148(19)	17.1(4)	25.348(10)	86.83(2)	84.38(2)	79.899(18)	4080(2)
253	9.6038(19)	17.09(4)	25.362(9)	86.82(2)	84.44(2)	79.792(19)	4074(2)
243	9.585(2)	17.073(4)	25.357(9)	86.69(2)	84.37(2)	79.656(18)	4059(2)
233	9.5716(18)	17.068(4)	25.38(8)	86.63(2)	84.4(2)	79.522(18)	4054(2)
223	9.5463(18)	17.047(4)	25.372(8)	86.6(2)	84.4(2)	79.427(17)	4036(2)
213	9.521(2)	17.025(4)	25.373(8)	86.59(2)	84.35(2)	79.315(18)	4018(2)
203	9.5187(18)	17.045(4)	25.463(8)	86.64(2)	84.34(2)	79.231(18)	4035(2)
193	9.4986(18)	17.017(5)	25.374(11)	86.68(3)	84.22(2)	79.11(2)	4004(2)
183	9.3385(12)	17.02(4)	25.679(6)	88.36(2)	83.105(15)	80.909(15)	4001(2)
173	9.3032(12)	16.994(3)	25.671(5)	88.558(15)	82.952(13)	81.092(13)	3979(1)
163	9.245(3)	16.907(7)	25.499(11)	88.92(4)	82.98(3)	81.2(3)	3909(3)
153	9.25(3)	16.905(7)	25.6(13)	89.07(4)	82.97(3)	81.34(3)	3928(3)
143	9.243(2)	16.949(7)	25.645(12)	89.06(4)	82.86(3)	81.34(3)	3941(3)
133	9.213(3)	16.879(8)	25.538(13)	89.24(4)	82.88(4)	81.38(3)	3896(3)
123	9.213(3)	16.905(8)	25.641(14)	89.18(4)	83.03(4)	81.49(3)	3920(3)
133	9.219(3)	16.896(7)	25.595(14)	89.2(4)	82.9(3)	81.34(3)	3911(3)
143	9.222(3)	16.902(7)	25.533(13)	89.14(4)	82.95(3)	81.4(3)	3906(3)
153	9.235(3)	16.909(7)	25.52(12)	89.03(4)	83(3)	81.35(3)	3910(3)
163	9.266(2)	16.936(8)	25.579(13)	88.92(4)	82.96(3)	81.2(3)	3937(3)
173	9.281(2)	16.932(10)	25.549(14)	88.99(5)	83.13(3)	81.24(3)	3939(3)
183	9.314(3)	16.917(8)	25.589(12)	88.48(4)	83.09(3)	81(3)	3953(3)
193	9.4794(15)	17.057(5)	25.572(7)	86.81(2)	84.053(18)	79.47(18)	4040(2)
203	9.5243(14)	17.081(3)	25.501(5)	86.48(16)	84.305(14)	79.236(14)	4052(1)
213	9.5416(14)	17.077(3)	25.448(5)	86.458(17)	84.356(14)	79.287(15)	4051(1)
223	9.5631(18)	17.07(4)	25.455(5)	86.561(17)	84.448(17)	79.41(17)	4062(1)
233	9.5791(18)	17.08(4)	25.436(6)	86.606(18)	84.45(17)	79.524(18)	4069(1)
243	9.6031(16)	17.12(4)	25.435(6)	86.616(18)	84.396(16)	79.577(16)	4089(1)
253	9.6099(17)	17.12(4)	25.411(5)	86.656(18)	84.359(16)	79.678(16)	4089(1)
263	9.6295(17)	17.128(4)	25.407(6)	86.731(18)	84.331(16)	79.842(16)	4101(1)
273	9.6365(17)	17.123(4)	25.365(6)	86.806(19)	84.306(17)	79.952(17)	4098(2)
283	9.6535(18)	17.143(4)	25.365(6)	86.89(2)	84.266(18)	80.062(18)	4111(2)
293	9.6783(18)	17.169(4)	25.386(6)	86.97(2)	84.246(18)	80.156(18)	4133(2)

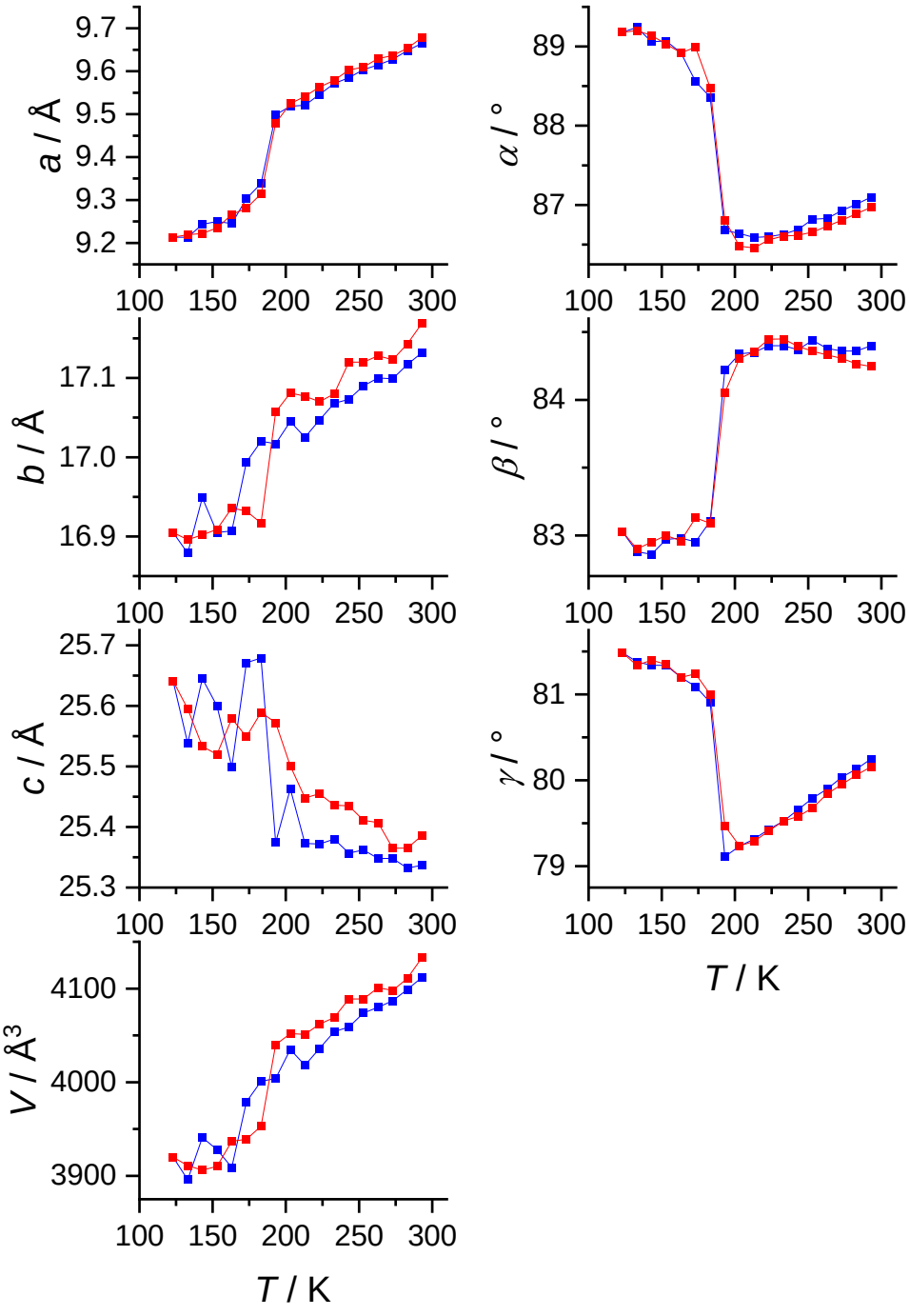

Fig. S6 *T*-dependence of the crystalline cell parameters for **1** in the cooling (blue) and heating (red) process.

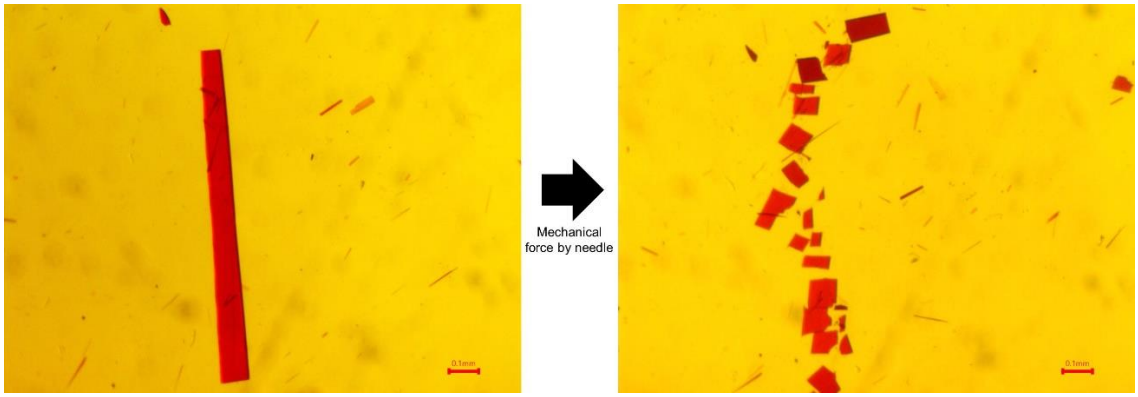

Fig. S7. Crystal of **1** (left) did not exhibit mechanically induced fibreization upon applying force by needle (right) as reported in the elastic crystals with similar packings.[6, 7] One possible explanation for the absence of fibreization is larger interactions between π-stacked columns due to dispersion interactions of the undecyl chains, that prevent cleavage along (0*kl*) planes. Figs. S8-S11 summarize the energy frameworks and interaction energies of the high-*T* (273 K) and low-*T* (123 K) phases of **1**. In both phases, intracolumn interactions (216-270 kJ mol^{-1}) are larger than those of the intercolumn interactions, indicating the anisotropic interaction topologies. The intercolumn interactions between adjacent pair of the molecules are larger than 100 kJ mol^{-1}, preventing the disassembly of π-stacked columns under mechanical stress.

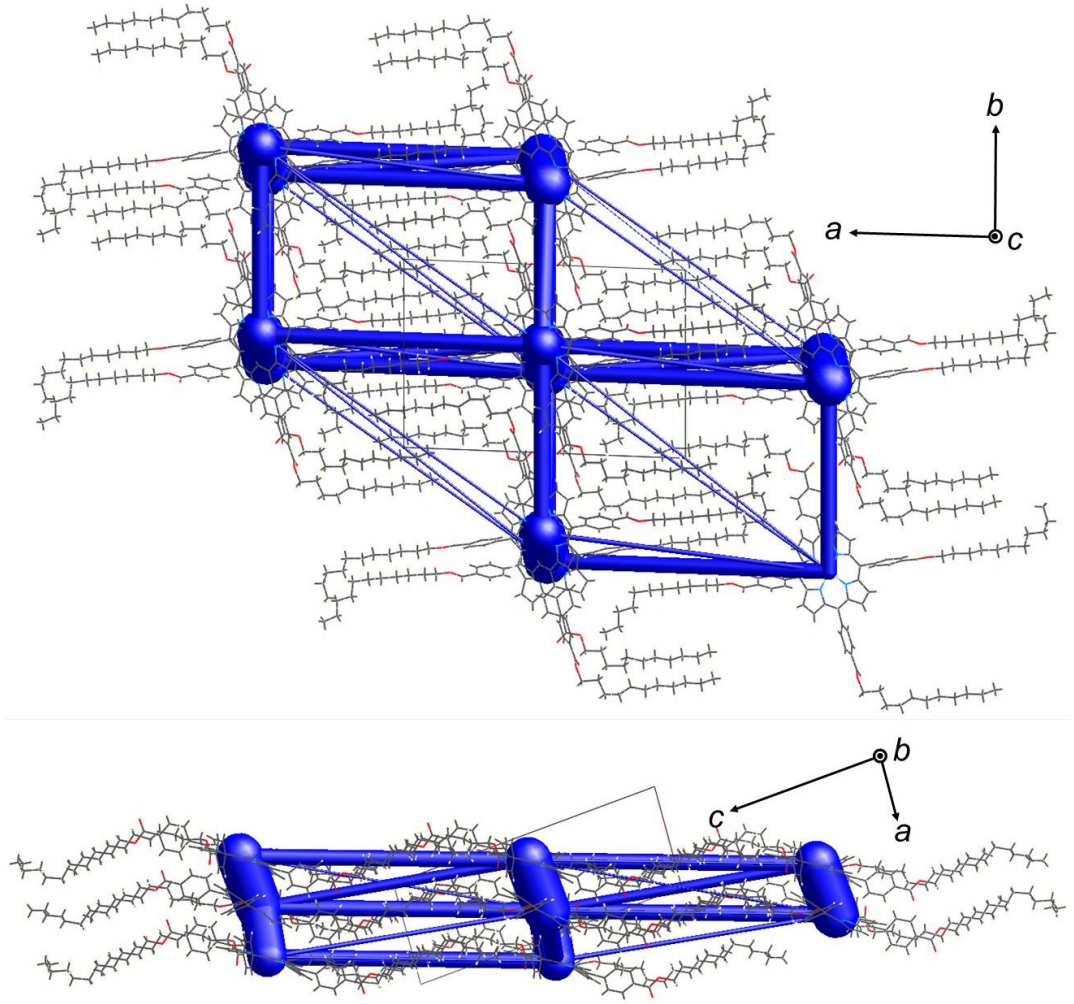

Fig. S8 Energy framework based on total interaction energy using SCXRD data at 273 K. One of the disordered conformations with the larger occupancy was used. Cu^{2+} ion was replaced by Ni^{2+} ion to avoid the effect of spin.

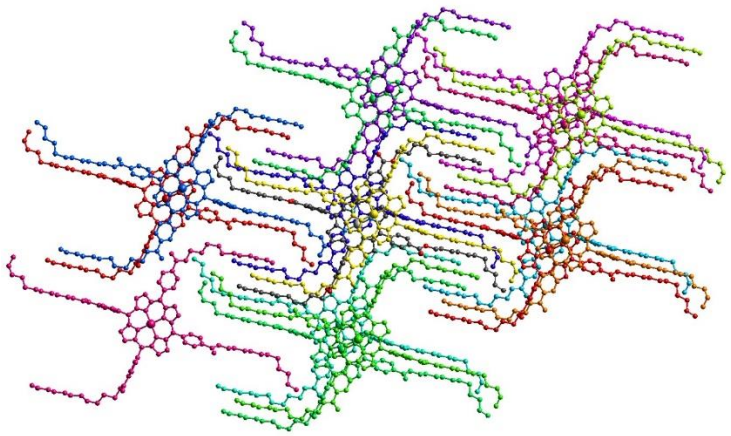

Interaction Energies (kJ/mol)
R is the distance between molecular centroids (mean atomic position) in Å.

Total energies, only reported for two benchmarked energy models, are the sum of the four energy components, scaled appropriately (see the scale factor table below)

N	Symop	R	Electron Density	E_ele	E_pol	E_dis	E_rep	E_tot
2	x, y, z	26.23	HF/3-21G	-0.7	-1.1	-94.7	0.0	-86.7
1	-x, -y, -z	28.47	HF/3-21G	-2.9	-0.2	-12.1	0.0	-14.0
1	-x, -y, -z	5.19	HF/3-21G	-42.1	-14.9	-349.3	140.7	-253.1
1	-x, -y, -z	33.91	HF/3-21G	1.7	-0.0	-7.2	0.0	-4.8
1	-x, -y, -z	16.23	HF/3-21G	-12.0	-9.3	-61.7	0.0	-73.8
2	x, y, z	17.10	HF/3-21G	34.0	-7.6	-134.6	0.0	-91.6
1	-x, -y, -z	14.57	HF/3-21G	11.9	-3.1	-124.4	0.0	-102.0
1	-x, -y, -z	26.04	HF/3-21G	2.0	-0.3	-31.6	0.0	-26.7
1	-x, -y, -z	24.89	HF/3-21G	1.9	-1.2	-67.7	0.0	-59.8
1	-x, -y, -z	5.67	HF/3-21G	-53.4	-13.1	-292.5	136.3	-216.0
1	-x, -y, -z	19.37	HF/3-21G	5.0	-1.2	-14.8	0.0	-9.1
1	-x, -y, -z	32.77	HF/3-21G	0.5	-0.1	-15.8	0.0	-13.8
2	x, y, z	31.17	HF/3-21G	5.3	-0.0	-21.6	0.0	-14.1

Scale factors for benchmarked energy models
See Mackenzie et al. IUCrJ (2017)

Energy Model	k_ele	k_pol	k_disp	k_rep
CE-HF .. HF/3-21G electron densities	1.019	0.651	0.901	0.811

Fig. S9 Interaction energies between pairs of the molecules using the SCXRD structure at 273 K.

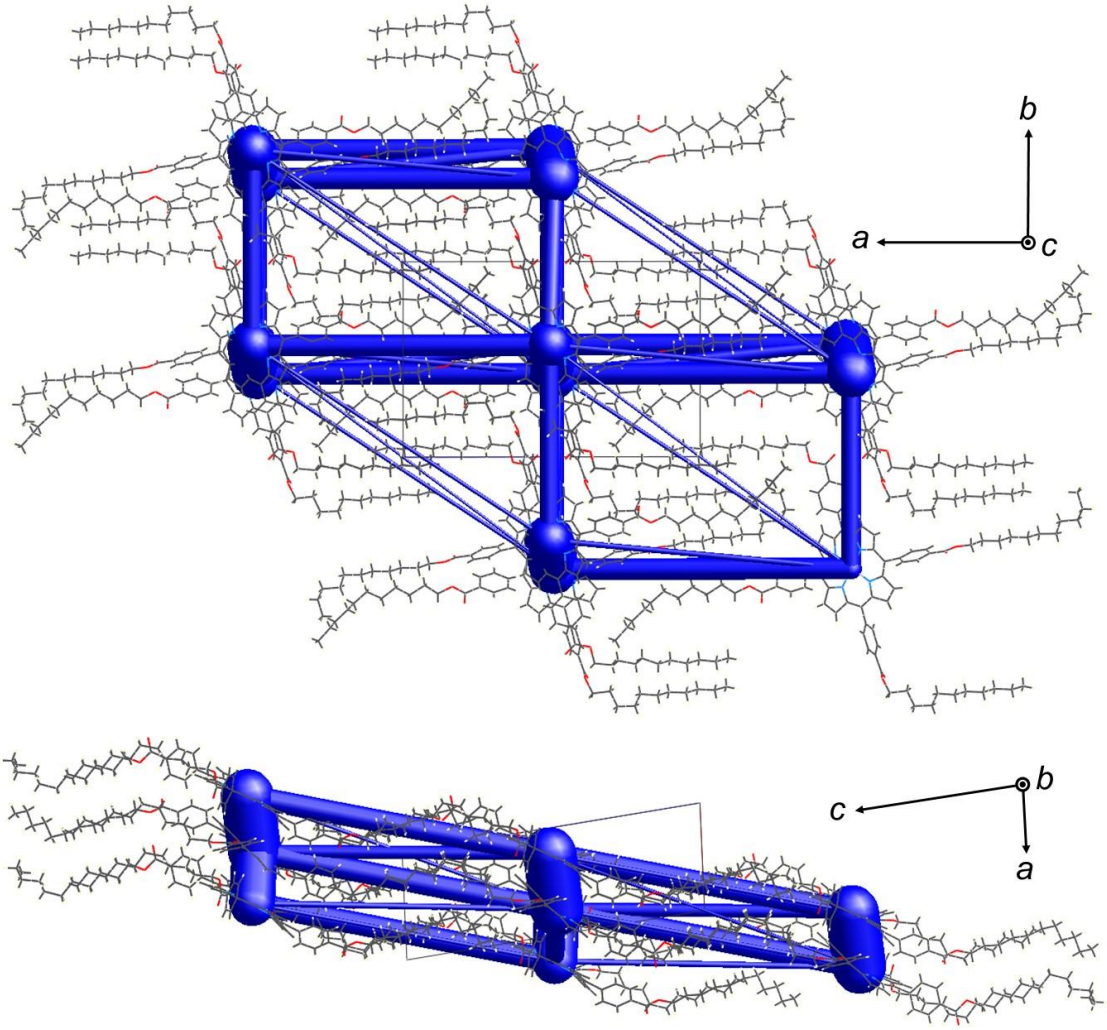

Fig. S10 Energy framework based on total interaction energy using SCXRD data at 123 K. Cu^{2+} ion was replaced by Ni^{2+} ion to avoid the effect of spin.

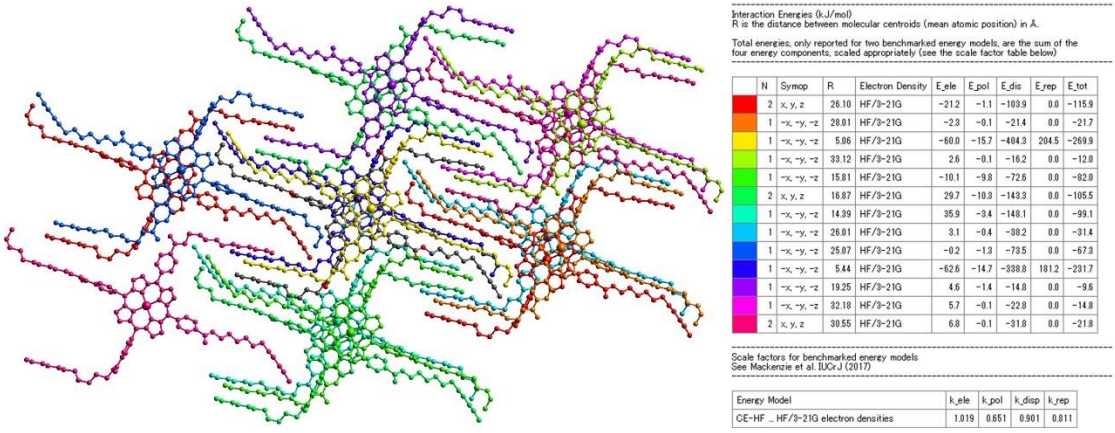

Interaction Energies (kJ/mol)
R is the distance between molecular centroids (mean atomic position) in Å.

Total energies, only reported for two benchmarked energy models, are the sum of the four energy components, scaled appropriately (see the scale factor table below)

N	Symop	R	Electron Density	E_ele	E_pol	E_dis	E_rep	E_tot
2	x, y, z	26.10	HF/3-21G	-21.2	-1.1	-103.9	0.0	-115.9
1	-x, -y, -z	28.01	HF/3-21G	-2.3	-0.1	-21.4	0.0	-21.7
1	-x, -y, -z	5.06	HF/3-21G	-60.0	-15.7	-404.3	204.5	-269.9
1	-x, -y, -z	33.12	HF/3-21G	2.6	-0.1	-16.2	0.0	-12.0
1	-x, -y, -z	15.81	HF/3-21G	-10.1	-9.8	-72.6	0.0	-82.0
2	x, y, z	16.87	HF/3-21G	29.7	-10.3	-143.3	0.0	-105.5
1	-x, -y, -z	14.39	HF/3-21G	35.9	-3.4	-148.1	0.0	-99.1
1	-x, -y, -z	26.01	HF/3-21G	3.1	-0.4	-38.2	0.0	-31.4
1	-x, -y, -z	25.97	HF/3-21G	-0.2	-1.3	-73.5	0.0	-67.3
1	-x, -y, -z	5.44	HF/3-21G	-62.6	-14.7	-338.8	181.2	-231.7
1	-x, -y, -z	19.25	HF/3-21G	4.6	-1.4	-14.8	0.0	-9.6
1	-x, -y, -z	32.18	HF/3-21G	5.7	-0.1	-22.8	0.0	-14.8
2	x, y, z	30.55	HF/3-21G	6.8	-0.1	-31.8	0.0	-21.8

Scale factors for benchmarked energy models
See Mackenzie et al. IUCrJ (2017)

Energy Model	k_ele	k_pol	k_disp	k_rep
CE-HF _ HF/3-21G electron densities	1.019	0.651	0.901	0.811

Fig. S11 Interaction energies between pairs of the molecules using the SCXRD structure at 123 K.

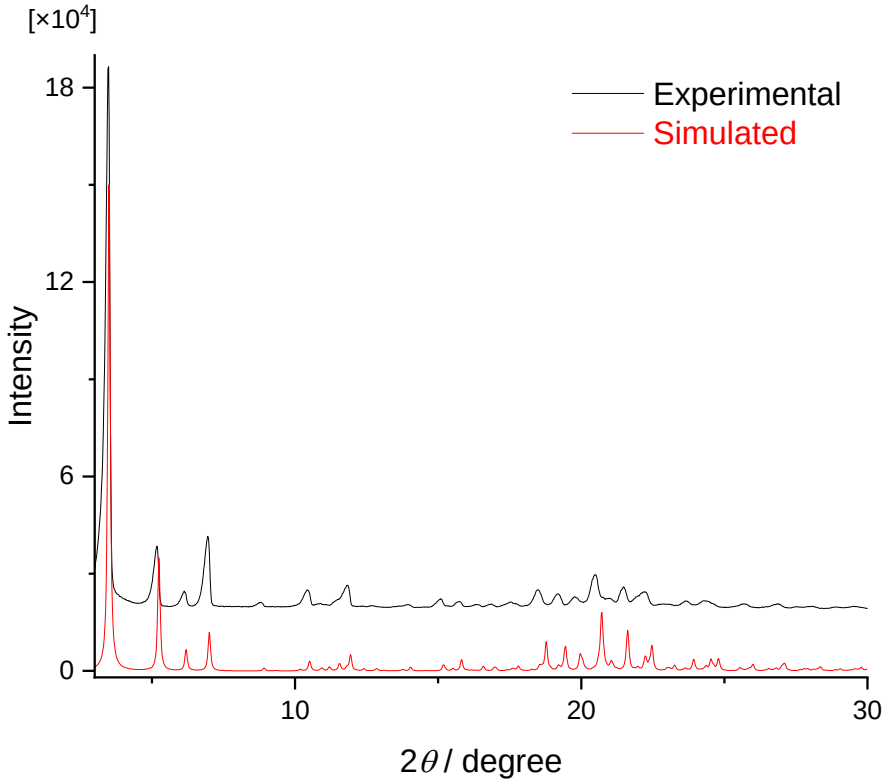

Fig. S12 PXRD patterns for **1**. Simulated pattern was derived from SCXRD data at 273 K.

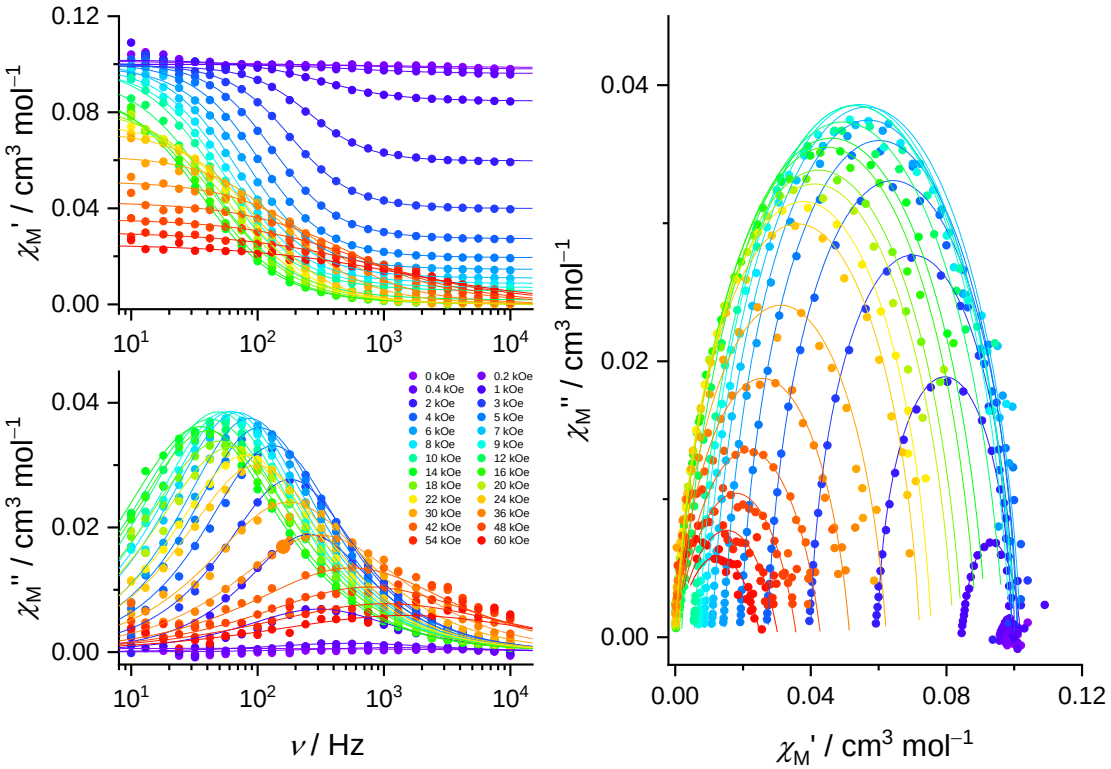

Fig. S13 *H*-dependence of the ac magnetic susceptibilities at T = 4 K.

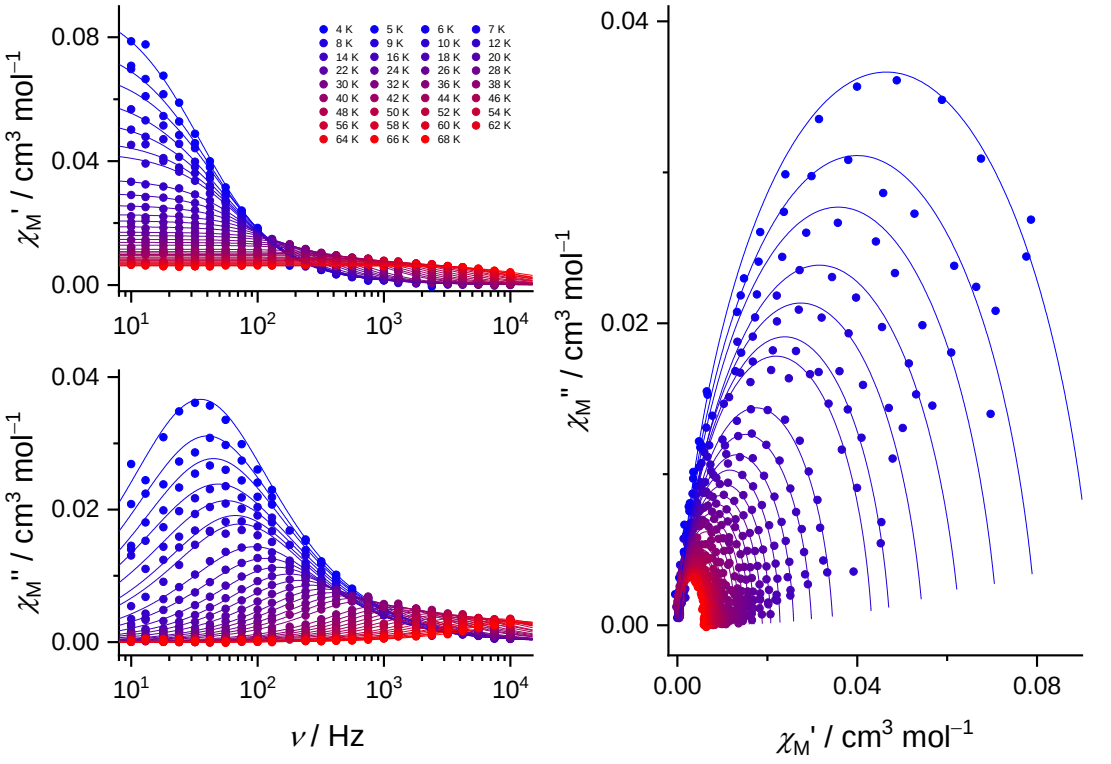

Fig. S14 *T*-dependence of the ac magnetic susceptibilities at H = 14 kOe.

References

1. G. Sheldrick, *Acta Crystallogr. A*, 2008, **64**, 112-122.
2. C. Kabuto, S. Akine, T. Nemoto and E. Kwon, *Nihon Kessho Gakkaishi*, 2009, **51**, 218-224.
3. C. F. Macrae, I. Sovago, S. J. Cottrell, P. T. A. Galek, P. McCabe, E. Pidcock, M. Platings, G. P. Shields, J. S. Stevens, M. Towler and P. A. Wood, *J. Appl. Crystallogr.*, 2020, **53**, 226-235.
4. T. H. J. Niedermeyer and M. Strohalm, *PLOS ONE*, 2012, **7**, e44913.
5. P. R. Spackman, M. J. Turner, J. J. McKinnon, S. K. Wolff, D. J. Grimwood, D. Jayatilaka and M. A. Spackman, *J. Appl. Crystallogr.*, 2021, **54**, 1006-1011.
6. S. Hayashi and T. Koizumi, *Chem. Eur. J.*, 2018, **24**, 8507-8512.
7. S. Kusumoto, A. Sugimoto, Y. Zhang, Y. Kim, M. Nakamura and S. Hayami, *Inorg. Chem.*, 2021, **60**, 1294-1298.